The nucleon thermal width due to pion-baryon loops and its contribution in Shear viscosity

Sabyasachi Ghosh
Instituto de Fisica Teorica, Universidade Estadual Paulista,
Rua Dr. Bento Teobaldo Ferraz, 271, 01140-070 Sao Paulo, SP, Brazil.

In the real-time thermal field theory, the standard expression of shear viscosity for the nucleonic constituents is derived from the two point function of nucleonic viscous stress tensors at finite temperature and density. The finite thermal width or Landau damping is traditionally included in the nucleon propagators. This thermal width is calculated from the in-medium self-energy of nucleon for different possible pion-baryon loops. The dynamical part of nucleon-pion-baryon interactions are taken care by the effective Lagrangian densities of standard hadronic model. The shear viscosity to entropy density ratio of nucleonic component decreases with the temperature and increases with the nucleon chemical potential. However, adding the contribution of pionic component, total viscosity to entropy density ratio also reduces with the nucleon chemical potential when the mixing effect between pion and nucleon components in the mixed gas is considered. Within the hadronic domain, viscosity to entropy density ratio of the nuclear matter is gradually reducing as temperature and nucleon chemical potential are growing up and therefore the nuclear matter is approaching toward the (nearly) perfect fluid nature.

I. INTRODUCTION

The recent hydrodynamical [1, 2] as well as some transport studies [3, 4] have indicated about an (nearly) ideal fluid nature of nuclear matter, which may be produced in the experiments of heavy ion collisions (HIC) like Relativistic Heavy Ion Collider (RHIC) at BNL. The hydrodynamical calculations became very successful in explaining the elliptical flow parameter, v_2 from RHIC data [5–7] only when they assumed a very small ratio of shear viscosity to entropy density (η/s) for the expanding nuclear matter. When some recent studies [8–11] (see also Ref. [12]) show that η/s may reach a minimum in the vicinity of a phase transition, then some special attentions are drawn to the smallness of this minimum value with respect to its lower bound ($\eta/s = \frac{1}{4\pi}$), commonly known as the KSS bound [13]. In this context, the temperature (T) dependence of η/s is taken into account in some recent hydrodynamical calculations [14–17] instead of its constant value during the entire evolution. Niemi *et al.* [14] have interestingly observed that the $v_2(p_T)$ of RHIC data is highly sensitive to the temperature dependent η/s in hadronic matter and almost independent of the viscosity in QGP phase. This work gives an additional boost to the microscopic calculations of η/s of the hadronic matter in the recent years [18–34], though historically these investigations are slightly old [35–40].

Except a few [24, 30–32], most of the microscopic calculations are done in zero baryon or nucleon chemical potential ($\mu_N = 0$). Along with the T dependence of η or η/s, their dependence on the baryon chemical potential should also be understood in view of the future experiments such as FAIR. In the work of Itakura *et al.* [24] and Denicol *et al.* [31], we notice that the η/s is reduced at finite baryon chemical potential, whereas Gorenstein *et al.* [30] observed an increasing nature of η/s with μ_N. Itakura *et al.* have obtained η by solving the relativistic quantum Boltzmann equation, where phenomenological amplitudes of hadrons are used in the collision terms. Denicol *et al.* have calculated the η at finite T and μ_N by applying Chapman-Enskog theory in Hadron Resonance Gas (HRG) model, whereas Gorenstein *et al.* have taken a simplified ansatz of η to estimate η/s in the van der Waals excluded volume HRG model. Similar to the ansatz of $\eta(T)$ taken by Gorenstein *et al.*, the η itself increases with increasing temperature in Ref. [24], but their η/s are exhibiting completely opposite nature of T dependence. Therefore, the behavior of the η/s may largely be influenced by the T dependence of entropy density s.

Motivating by these delicate issues of shear viscosity at finite μ_N, the present manuscript is concentrated on the matter with nucleon degrees of freedom at finite T and μ_N. The nucleons in the medium can slightly become off-equilibrium because of their thermal width or Landau damping, which can be originated from the nucleon thermal fluctuations into different baryons and pion. The inverse of nucleon thermal width measures the relaxation time of nucleon in the matter from which one can estimate its corresponding shear viscosity contribution.

In the next section, the one-loop expression of η for nucleon degrees of freedom is derived from the Kubo relation, where a finite thermal width is traditionally included in the nucleon propagators. This standard expression of η can also be deduced from relaxation time approximation of kinematic theory approach. In the real-time thermal field theory, the nucleon thermal width from the different pion-baryon loops are calculated in Sec. 3, where their interactions are determined from the effective hadronic model. In Sec. 4, the numerical results are discussed followed by summary and conclusions in Sec. 5.

II. KUBO RELATION FOR SHEAR VISCOSITY OF NUCLEAR MATTER

From the simple derivation of Kubo formula [41, 42], let us start with the expression of shear viscosity for nucleonic constituents in momentum space [26, 46],

$$\eta_N = \frac{1}{20}\lim_{q_0,\vec{q}\to 0}\frac{A_\eta(q_0,\vec{q})}{q_0}\ , \tag{1}$$

where

$$A_\eta(q_0,\vec{q}) = \int d^4x e^{iq\cdot x}\langle[\pi_{\mu\nu}(x),\pi^{\mu\nu}(0)]\rangle_\beta \tag{2}$$

is the spectral representation of two point function for nucleonic viscous-stress tensor, $\pi^{\mu\nu}$ and

$$\langle\hat{O}\rangle_\beta = \mathrm{Tr}\frac{e^{-\beta H}\hat{O}}{Z} \quad \text{with} \quad Z = \mathrm{Tr}e^{-\beta H} \tag{3}$$

is denoting the thermodynamical ensemble average. The energy momentum tensor of free nucleon is

$$\begin{aligned} T_{\rho\sigma} &= -g_{\rho\sigma}\mathcal{L} + \frac{\partial\mathcal{L}}{\partial(\partial^\rho\psi)}\partial_\sigma\psi \\ &= -g_{\rho\sigma}\mathcal{L} + i\overline{\psi}\gamma_\rho\partial_\sigma\psi\ , \end{aligned} \tag{4}$$

and hence the viscous stress tensor will be

$$\begin{aligned} \pi_{\mu\nu} &= t^{\rho\sigma}_{\mu\nu}T_{\rho\sigma} \\ &= t^{\rho\sigma}_{\mu\nu}i\overline{\psi}\gamma_\rho\partial_\sigma\psi \ \ (\text{ since } t^{\rho\sigma}_{\mu\nu}g_{\rho\sigma}=0\ )\ , \end{aligned} \tag{5}$$

where

$$t^{\rho\sigma}_{\mu\nu} = \Delta^\rho_\mu\Delta^\sigma_\nu - \frac{1}{3}\Delta_{\mu\nu}\Delta^{\rho\sigma},\ \ \Delta^{\mu\nu} = g^{\mu\nu} - u^\mu u^\nu\ . \tag{6}$$

In real-time formalism of thermal field theory, the ensemble average of any two point function always becomes a 2×2 matrix structure. Hence, for viscous-stress tensor, the matrix structure of two point function becomes

$$\Pi_{ab}(q) = i\int d^4x e^{iqx}\langle T_c\pi_{\mu\nu}(x)\pi^{\mu\nu}(0)\rangle^{ab}_\beta\ , \tag{7}$$

where the superscripts $a, b (a, b = 1, 2)$ denote the thermal indices of the matrix and T_c denotes time ordering with respect to a symmetrical contour [43, 44] in the complex time plane.

The matrix can be diagonalized in terms of a single analytic function, which can also be related with the retarded two point function of viscous-stress tensor. The retarded function $\Pi^R(q)$, diagonal element $\overline{\Pi}(q)$ and the spectral function $A_\eta(q)$ are simply related to any one of the components of $\Pi_{ab}(q)$. Their relations with 11 component is given below

$$\begin{aligned} A_\eta(q) &= 2\mathrm{Im}\Pi^R(q) = 2\epsilon(q_0)\mathrm{Im}\overline{\Pi}(q) \\ &= 2\tanh(\frac{\beta q_0}{2})\mathrm{Im}\Pi_{11}(q)\ . \end{aligned} \tag{8}$$

Hence, Eq. (1) can broadly be redefined as

$$\begin{aligned} \eta_N &= \frac{1}{10}\lim_{q_0,\vec{q}\to 0}\frac{\mathrm{Im}\Pi^R(q_0,\vec{q})}{q_0} = \frac{1}{10}\lim_{q_0,\vec{q}\to 0}\frac{\epsilon(q_0)\mathrm{Im}\overline{\Pi}(q_0,\vec{q})}{q_0} \\ &= \frac{1}{10}\lim_{q_0,\vec{q}\to 0}\frac{\tanh(\beta q_0/2)\mathrm{Im}\Pi^{11}(q_0,\vec{q})}{q_0}\ . \end{aligned} \tag{9}$$

Using (5) in the 11 component of (7) and then applying the Wick's contraction technique, we have

$$\begin{aligned} \Pi_{11}(q) &= t^{\rho\sigma}_{\alpha\beta}t^{\alpha\beta}_{\mu\nu}i\int d^4x e^{iqx}\langle T\overline{\psi}(x)\gamma_\rho\partial_\sigma\psi\overbrace{(x)\overline{\psi}}(0)\gamma^\mu\partial^\nu\psi(0)\rangle_\beta \\ &= i\int\frac{d^4k}{(2\pi)^4}N(q,k)D_{11}(k)D_{11}(p=q+k)\ , \end{aligned} \tag{10}$$

where

$$N(q,k) = -I_N t^{\rho\sigma}_{\mu\nu}\mathrm{Tr}[\gamma^\mu(q+k)^\nu(\not{q}+\not{k}+m_N)\gamma_\rho k_\sigma(\not{k}+m_N)]\ . \tag{11}$$

This self-energy function, $\Pi_{11}(q)$ for NN loop can diagrammatically be represented by Fig. 1(A). In the co-moving frame, *i.e.*, for $u = (1,\vec{0})$, the $N(q,k)$ becomes

$$\begin{aligned} N(q,k) &= -I_N\left[\frac{32}{3}\{k_0(q_0+k_0)\}\{\vec{k}\cdot(\vec{q}+\vec{k})\}\right. \\ &\quad \left.-4\left[\{\vec{k}\cdot(\vec{q}+\vec{k})\}^2 + \frac{\vec{k}^2(\vec{q}+\vec{k})^2}{3}\right]\right]\ . \end{aligned} \tag{12}$$

In the above equations, $I_N = 2$ is the isospin degeneracy of nucleon.

In Eq. (10), D^{11} is scalar part of 11 component of the nucleon propagator at finite temperature and density. Its form is

$$\begin{aligned} D^{11}(k) &= \frac{-1}{k^2 - m_N^2 + i\eta} - 2\pi i F_k(k_0)\delta(k^2 - m_N^2) \\ &\text{with}\ \ F_k(k_0) = n_k^+\theta(k_0) + n_k^-\theta(-k_0) \\ &= -\frac{1}{2\omega_k^N}\Big(\frac{1-n_k^+}{k_0-\omega_k^N+i\eta} + \frac{n_k^+}{k_0-\omega_k^N-i\eta} \\ &\quad - \frac{1-n_k^-}{k_0+\omega_k^N-i\eta} - \frac{n_k^-}{k_0+\omega_k^N+i\eta}\Big), \end{aligned} \tag{13}$$

where $n_k^\pm(\omega_k^N) = 1/\{e^{\beta(\omega_k^N\mp\mu_N)}+1\}$ is Fermi-Dirac distribution function for energy $\omega_k^N = \sqrt{\vec{k}^2+m_N^2}$. Here the $\pm$ signs in the superscript of n_k stand for nucleon and anti-nucleon respectively. Among the four terms in Eq. (13), the first and the second terms are associated with the nucleon propagation above the Fermi sea and the propagation of its hole in the Fermi sea respectively, while the third and fourth terms represent the corresponding situations for anti-nucleon. The full relativistic nucleon propagator, thus, treats the particle and anti-particle on an equal footing and all possible singularities (nucleon, hole of the nucleon, anti-nucleon and hole of the anti-nucleon) are automatically included.

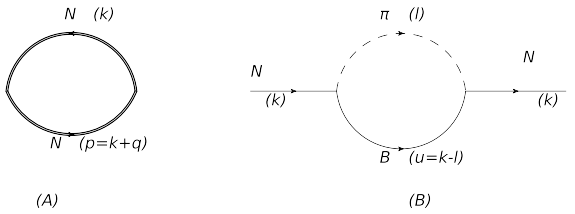

FIG. 1: Diagrammatic representation of NN loop is shown in (A), where double lines stand for effective N propagators, which contain their thermal widths Γ. The diagrammatic representation of nucleon self-energy for πB loop is shown in (B) from where Γ can be determined.

After doing the k_0 integration of Eq. (10) and then using it in Eq. (9), we have

$$\eta_N = \frac{1}{10}\lim_{q_0,\vec{q}\to 0}\int\frac{d^3k}{(2\pi)^3}\frac{(-\pi N)}{4\omega_k^N\omega_p^N} \left[\frac{\{-n_k^-(\omega_k^N)+n_p^-(-q_0+\omega_k^N)\}}{q_0}\delta(q_0-\omega_k^N+\omega_p^N) + \frac{\{n_k^+(\omega_k^N)-n_p^+(q_0+\omega_k^N)\}}{q_0}\delta(q_0+\omega_k^N-\omega_p^N)+..\right] \quad (14)$$

where $N = N(k_0 = \pm\omega_k^N, \vec{k}, q)$ and $\omega_p^N = \sqrt{(\vec{q}+\vec{k})^2+m_N^2}$.

The two δ-functions will be responsible for generating the Landau cuts ($-\vec{q} < q_0 < \vec{q}$), where the $\mathrm{Im}\Pi^R(q)$ will be non-zero. However, there will be two more δ-functions (not written explicitly), which are not important for the limiting point $q_0, \vec{q} \to 0$ since they will generate unitary cuts ($-\infty < q_0 < -\sqrt{\vec{q}^2+4m_N^2}$ and $\sqrt{\vec{q}^2+4m_N^2} < q_0 < \infty$).

Using the identity

$$-\pi\delta(x) = \mathrm{Im}\left[\lim_{\Gamma_N\to 0}\frac{1}{x+i\Gamma_N}\right] \quad (15)$$

in Eq. (14), we have

$$\eta_N = \frac{1}{10}\lim_{q_0,\vec{q}\to 0}\mathrm{Im}\left[\int\frac{d^3k}{(2\pi)^3}\frac{N}{4\omega_k^N\omega_p^N}\lim_{\Gamma_N\to 0} \left\{\frac{\{-n_k^-(\omega_k^N)+n_p^-(-q_0+\omega_k^N)\}/q_0}{(q_0-\omega_k^N+\omega_p^N)+i\Gamma_N} + \frac{\{n_k^+(\omega_k^N)-n_p^+(q_0+\omega_k^N)\}/q_0}{(q_0+\omega_k^N-\omega_p^N)+i\Gamma_N}\right\}\right] . \quad (16)$$

We will continue our further calculation for finite value of Γ_N to get a non-divergent contribution of η_N. Including thermal width Γ_N for constituent particles (here nucleons) of the medium is a very well established technique [26, 27, 45] in Kubo approach to remove the divergence of η_N as well as to incorporate the interaction scenario, which is very essential for a dissipative system. The interaction scenario is coming into the picture by transforming the delta functions to the spectral functions with finite thermal width. The thermal width (or collision rate) Γ_N of the constituent particles reciprocally measures the shear viscosity coefficient, which is approximately equivalent to the quasi particle description.

In the limiting case of $q_0, \vec{q} \to 0$, we get $\omega_p^N \to \omega_k^N$ and therefore Eq. (16) is transformed to

$$\eta_N = \frac{1}{10}\int\frac{d^3k}{(2\pi)^3}\frac{(-N_0)}{4{\omega_k^N}^2\Gamma_N}\left[I_2+I_3\right] , \quad (17)$$

where

$$N_0 = \lim_{q_0,\vec{q}\to 0} N(k_0 = \pm\omega_k^N, \vec{k}, q) \quad (18)$$

and

$$I_{2,3} = \lim_{q_0\to 0}\frac{\{\mp n_k^\mp(\omega_k^N) \pm n_p^\mp(\mp q_0+\omega_k^N)\}}{q_0} . \quad (19)$$

In the above Eq. (19), one can notice that the limiting value of $I_{2,3}$ is of the 0/0 form. Therefore, we can apply the L'Hospital's rule, *i.e.*,

$$I_{2,3} = \lim_{q_0\to 0}\frac{\frac{d}{dq_0}\{\mp n_k^\mp(\omega_k^N) \pm n_p^\mp(\mp q_0+\omega_k^N)\}}{\frac{d}{dq_0}\{q_0\}} = \beta[n_k^\mp(1-n_k^\mp)] , \quad (20)$$

since

$$\frac{d}{dq_0}\{\pm n_p^\mp(\omega_q = \mp q_0+\omega_k^N)\} = \pm\frac{-\beta\frac{d\omega_q}{dq_0}e^{\beta(\omega_q\pm\mu_N)}}{\{e^{\beta(\omega_q\pm\mu_N)}+1\}^2}$$

$$\lim_{q_0\to 0}\frac{d}{dq_0}\{\pm n_p^\mp(\omega_q = \mp q_0+\omega_k^N)\} = \pm\frac{-(\mp)\beta e^{\beta(\omega_k^N\pm\mu_N)}}{\{e^{\beta(\omega_k^N\pm\mu_N)}+1\}^2} = \beta[n_k^\mp(1-n_k^\mp)] . \quad (21)$$

Again, in the limiting value of $q_0, \vec{q} \to 0$, Eq. (12) can be simplified to

$$N^0 = -I_N\frac{16\vec{k}^4}{3} . \quad (22)$$

Hence, using the above results, the Eq. (17) becomes

$$\eta_N = \frac{8\beta I_N}{15}\int\frac{d^3k}{(2\pi)^3}\frac{\vec{k}^4}{4{\omega_k^N}^2\Gamma_N}\left[n_k^-(1-n_k^-)+n_k^+(1-n_k^+)\right] = \frac{\beta I_N}{15\pi^2}\int\frac{\vec{k}^6 d\vec{k}}{{\omega_k^N}^2\Gamma_N}[n_k^-(1-n_k^-)+n_k^+(1-n_k^+)] . \quad (23)$$

This is the one-loop expression of shear viscosity for the matter with nucleon degrees of freedom in the Kubo approach. Though there are possibility of infinite number of ladder-type diagrams, which are supposed to be of same order of magnitude ($\mathcal{O}(1/\Gamma_N)$) like the one-loop, they

Baryons	J_B^P	I_B	$\Gamma_{\rm tot}$	$\Gamma_{B\to N\pi}$ (B.R.)	f/m_π
$\Delta^(1232)$	$\frac{3}{2}^+$	3/2	0.117	0.117 (100%)	15.7
$N^*(1440)$	$\frac{1}{2}^+$	1/2	0.300	0.195 (65%)	2.5
$N^*(1520)$	$\frac{3}{2}^-$	1/2	0.115	0.069 (60%)	11.6
$N^*(1535)$	$\frac{1}{2}^-$	1/2	0.150	0.068 (45%)	1.14
$\Delta^*(1600)$	$\frac{3}{2}^+$	3/2	0.320	0.054 (17%)	3.4
$\Delta^*(1620)$	$\frac{1}{2}^-$	3/2	0.140	0.035 (25%)	1.22
$N^*(1650)$	$\frac{1}{2}^-$	1/2	0.150	0.105 (70%)	1.14
$\Delta^*(1700)$	$\frac{3}{2}^-$	3/2	0.300	0.045 (15%)	9.5
$N^*(1700)$	$\frac{3}{2}^-$	1/2	0.100	0.012 (12%)	2.8
$N^*(1710)$	$\frac{1}{2}^+$	1/2	0.100	0.012 (12%)	0.35
$N^*(1720)$	$\frac{3}{2}^+$	1/2	0.250	0.028 (11%)	1.18

TABLE I: From the left to right columns, the table contain the baryons, their spin-parity quantum numbers J_B^P, isospin I_B, total decay width $\Gamma_{\rm tot}$, decay width in $N\pi$ channels $\Gamma_{B\to N\pi}$ or $\Gamma_B(m_B)$ in Eq. (32) (brackets displaying its Branching Ratio) and at the last coupling constants f/m_π.

will be highly suppressed [46]. As we increase the number of loops, the number of extra thermal distribution functions will also appear in the shear viscosity expression and hence their numerical suppression will successively grow. On this basis, the one-loop results may be considered as a leading order results. One can derive exactly same expression from relaxation time approximation in kinetic theory approach.

III. CALCULATION OF NUCLEON THERMAL WIDTH

Now, our next aim is to calculate the thermal width of nucleon Γ_N, which can be estimated from the retarded component of nucleon self-energy (Σ^R) at finite temperature and density. Their relation is given by

$$\Gamma_N(\vec{k},T,\mu_N) = -{\rm Im}\Sigma^R(k_0=\omega_k^N,\vec{k},T,\mu_N)\ . \qquad (24)$$

During the propagation in the hot and dense nuclear matter, nucleon may pass through different πB loops, where B stand for different higher mass baryons including nucleon itself. In this work, all possible 4-star baryon resonances with spin 1/2 and 3/2 are considered. These are $N(980)$, $\Delta(1232)$, $N^*(1440)$, $N^*(1520)$, $N^*(1535)$, $\Delta^*(1600)$, $\Delta^*(1620)$, $N^*(1650)$, $\Delta^*(1700)$, $N^*(1700)$, $N^*(1710)$ and $N^*(1720)$, where masses (in MeV) of the baryons are given inside the brackets. The nucleon self-energy for πB loop is shown in diagram 1(B) and its 11 component can be expressed as

$$\begin{aligned}\Sigma^{11}(k,T,\mu_N) &= -i\int\frac{d^4l}{(2\pi)^4}L(k,l)D_{11}(l,m_\pi,T)\\ &\quad D_{11}(u=k-l,m_B,T,\mu_N)\ , \qquad (25)\end{aligned}$$

where $D_{11}(l,m_\pi,T)$, $D_{11}(u=k-l,m_B,T,\mu_N)$ are scalar part of pion and baryon propagators at finite temperature and density. The $L(k,l)$ contains vertices and numerator parts of the propagators. The chemical potential of all baryons are assumed to be the same as nucleon chemical potential μ_N. Similar to Eq. (8), this 11 component is also related with retarded component as

$${\rm Im}\Sigma^R(k) = \coth\left\{\frac{\beta(k_0-\mu_N)}{2}\right\}{\rm Im}\Sigma_{11}(k)\ . \qquad (26)$$

Performing the l_0 integration in (25) and then using the relation (26), we get the imaginary part of retarded self-energy,

$$\begin{aligned}{\rm Im}\Sigma^R(k) &= \pi\int\frac{d^3l}{(2\pi)^3}\frac{1}{4\omega_l^\pi\omega_u^B}[L(l_0=\omega_l^\pi,\vec{l},k)\\ &\quad[\{1+n_l(\omega_l^\pi)-n_u^+(k_0-\omega_l^\pi)\}\delta(k_0-\omega_l^\pi-\omega_u^B)\\ &\quad+\{-n_l(\omega_l^\pi)-n_u^-(-k_0+\omega_l^\pi)\}\delta(k_0-\omega_l^\pi+\omega_u^B)]\\ &\quad+L(l_0=-\omega_l^\pi,\vec{l},k)[\{n_l(\omega_l^\pi)\\ &\quad+n_u^+(k_0+\omega_l^\pi)\}\delta(k_0+\omega_l^\pi-\omega_u^B)+\{-1\\ &\quad-n_l(\omega_l^\pi)+n_u^-(-k_0-\omega_l^\pi)\}\delta(k_0+\omega_l^\pi+\omega_u^B)]]\ , \qquad (27)\end{aligned}$$

where $\omega_u^B=\sqrt{(\vec{k}-\vec{l})^2+m_B^2}$, $n_u^\pm$ and n_l are respectively Fermi-Dirac and Bose-Einstein distribution functions. The regions of different branch cuts in k_0-axis are ($-\infty$ to $-\sqrt{\vec{k}^2+(m_\pi+m_B)^2}$) for unitary cut in negative k_0-axis, ($-\sqrt{\vec{k}^2+(m_B-m_\pi)^2}$ to $\sqrt{\vec{k}^2+(m_B-m_\pi)^2}$) for Landau cut and ($\sqrt{\vec{k}^2+(m_\pi+m_B)^2}$ to ∞) for unitary cut in positive k_0-axis. These are representing the different kinematic regions where the imaginary part of the nucleon self-energy becomes non-zero because of the different δ functions in Eq. (27). The Γ_N for all πB loops (except the πN) are coming from the Landau cut contribution associated with the third term of Eq. (27), which can be simplified as

$$\begin{aligned}\Gamma_N &= \frac{1}{16\pi\vec{k}}\int_{\widetilde{\omega}^+}^{\widetilde{\omega}^-}d\widetilde{\omega}\{n_l(\widetilde{\omega})+n_u^+(\omega_k^N+\widetilde{\omega})\}\\ &\quad L(l_0=-\widetilde{\omega},\vec{l}=\sqrt{\widetilde{\omega}^2-m_\pi^2},k_0=\omega_k^N,\vec{k})\ ,(28)\end{aligned}$$

where $n_l(\widetilde{\omega}) = 1/\{e^{\beta\widetilde{\omega}} - 1\}$, $n_u^+(\omega_k^N + \widetilde{\omega}) = 1/\{e^{\beta(\widetilde{\omega}+\omega_k^N-\mu_N)} + 1\}$, $\widetilde{\omega}^\pm = \frac{R^2}{2m_N^2}(-\omega_k^N \pm \vec{k}W)$ with $W = \sqrt{1-\frac{4m_\pi^2 m_N^2}{R^4}}$ and $R^2 = m_N^2 + m_\pi^2 - m_B^2$.

The effective Lagrangian densities for $BN\pi$ interactions are given below [47]

$$\mathcal{L} = \frac{f}{m_\pi}\overline{\psi}_B\gamma^\mu \left\{ \begin{array}{c} i\gamma^5 \\ \mathbb{1} \end{array} \right\} \psi_N \partial_\mu \pi + \text{h.c. for } J_B^P = \frac{1}{2}^\pm ,$$
$$\mathcal{L} = \frac{f}{m_\pi}\overline{\psi}_B^\mu \left\{ \begin{array}{c} \mathbb{1} \\ i\gamma^5 \end{array} \right\} \psi_N \partial_\mu \pi + \text{h.c. for } J_B^P = \frac{3}{2}^\pm , \quad (29)$$

where coupling constants f/m_π for different baryons have been fixed from their experimental vacuum widths in $N\pi$ channel. With the help of the above Lagrangian densities, one can easily find

$$\begin{aligned} L(k,l) &= -\left(\frac{f}{m_\pi}\right)^2 \not{l}(\not{k}-\not{l}-Pm_B)\not{l} \qquad \text{for } J_B^P = \frac{1}{2}^\pm , \\ L(k,l) &= -\left(\frac{f}{m_\pi}\right)^2 (\not{k}-\not{l}+Pm_B) l_\mu l_\nu \Big\{ -g^{\mu\nu} + \frac{1}{3}\gamma^\mu\gamma^\nu \\ &\quad + \frac{2}{3m_B^2}(k-l)^\mu (k-l)^\nu \\ &\quad + \frac{1}{3m_B}(\gamma^\mu (k-l)^\nu - (k-l)^\mu \gamma^\nu) \Big\} \text{ for } J_B^P = \frac{3}{2}^\pm . \end{aligned} \quad (30)$$

For simplification the coefficients of γ^0 and $\mathbb{1}$ are taken as in Ref. [48] and their addition gives

$$\begin{aligned} L(k,l) &= -\left(\frac{f}{m_\pi}\right)^2 \Big\{ \left(\frac{R^2}{2} - m_\pi^2\right) l_0 \\ &\quad - Pm_\pi^2 m_B \Big\} \text{ for } \qquad J_B^P = \frac{1}{2}^\pm , \\ L(k,l) &= -\left(\frac{f}{m_\pi}\right)^2 \frac{2}{3m_B^2} \Big\{ \left(\frac{R^2}{2} - m_\pi^2\right)^2 \\ &\quad - m_\pi^2 m_B^2 \Big\} (k_0 - l_0 + Pm_B) \text{ for } J_B^P = \frac{3}{2}^\pm . \end{aligned} \quad (31)$$

The isospin part of the Lagrangian densities are not written in the Eq. (29). The isospin structure for $J_B^P = \frac{1}{2}^\pm$ and $J_B^P = \frac{3}{2}^\pm$ should be $\overline{\psi}\vec{\tau}\cdot\vec{\pi}\psi$ and $\overline{\psi}\vec{T}\cdot\vec{\pi}\psi$ respectively, where $\vec{T}$ is the spin 3/2 transition operator and $\vec{\tau}$ is the Pauli operator. This issue is managed by multiplying appropriate isospin factors with the expressions of corresponding loop diagrams. The isospin factor for πN or πN^* loop is $I_{N\to\pi N,N^*} = 3$, whereas for the $\pi\Delta$ or $\pi\Delta^*$ loop, $I_{N\to\pi\Delta,\Delta^*} = 2$.

All baryon resonances have finite vacuum width in $N\pi$ decay channel. The calculations of these decay widths are very essential in the present work for two reasons. First is to fix the coupling constants f/m_π for different $BN\pi$ interaction Lagrangian densities and second is to include the effect of these baryon widths (Γ_B) on the nucleon thermal width Γ_N. Using the Lagrangian densities, the vacuum decay width of baryons B for $N\pi$ channel can be obtained as

$$\begin{aligned} \Gamma_B(m_B) &= \frac{I_{N^*\to\pi N}}{2J_B+1}\left(\frac{f}{m_\pi}\right)^2 \frac{|\vec{p}_{cm}|}{2\pi m_B}[2m_B|\vec{p}_{cm}|^2 \\ &\quad + m_\pi^2(\omega_{cm}^N - Pm_N)] \text{ for } J_B^P = \frac{1}{2}^\pm , \\ \Gamma_B(m_B) &= \frac{I_{\Delta,\Delta^*\to\pi N}}{2J_B+1}\left(\frac{f}{m_\pi}\right)^2 \frac{|\vec{p}_{cm}|^3}{3\pi m_B} \\ &\quad [\omega_{cm}^N + Pm_N] \text{ for } \qquad J_B^P = \frac{3}{2}^\pm , \end{aligned} \quad (32)$$

where $|\vec{p}_{cm}| = \frac{\sqrt{\{m_B^2-(m_N+m_\pi)^2\}\{m_B^2-(m_N-m_\pi)^2\}}}{2m_B}$ and $\omega_{cm}^N = \sqrt{|\vec{p}_{cm}|^2 + m_N^2}$. The isospin factors are $I_{N^*\to\pi N} = 3$ and $I_{\Delta,\Delta^*\to\pi N} = 1$ for the $N\pi$ decay channels of N^* and Δ^* (or Δ) respectively.

Now, the Γ_N in Eq. (28) can be convoluted (see *e.g.* Refs. [49, 50]) as

$$\begin{aligned} \Gamma_N(m_B) &= \frac{1}{N_B}\int_{m_B-2\Gamma_B(m_B)}^{m_B+2\Gamma_B(m_B)} dM_B A_B(M_B)\Gamma_N(M_B) , \\ N_B &= \int_{m_B-2\Gamma_B(m_B)}^{m_B+2\Gamma_B(m_B)} A_B(M_B) , \end{aligned} \quad (33)$$

where

$$A_B(M_B) = \frac{1}{\pi}\text{Im}\left[\frac{1}{M_B - m_B + i\Gamma_B(M_B)/2}\right] \quad (34)$$

is vacuum spectral function of baryons for their vacuum decay width in $N\pi$ channel. Replacing baryon mass m_B by its invariant mass M_B in Eq. (32), one can get the off-mass shell expression of $\Gamma_B(M)$. The values of coupling constants f/m_π, which are fixed from the experimental values of baryon decay width in $N\pi$ channels [51], are shown in a Table (I).

IV. RESULTS AND DISCUSSION

Let us first take a glance at the invariant mass distribution of imaginary part of nucleon self-energy for different πB loops. Fig. (2) shows the results for baryons $B = N(940)$, $\Delta(1232)$ (upper panel) and $B = \Delta^*(1620)$, $N^*(1650)$, $N^*(1720)$ (lower panel), whereas Fig. (3) displays the results for baryons $B = N^*(1440)$, $N^*(1520)$, $\Delta^*(1600)$ (upper panel) and $B = N^*(1535)$, $\Delta^*(1700)$ (lower panel). The numerical strengths for $B = N^*(1700)$ and $N^*(1710)$ are too low to display with the other baryons. These results are obtained by replacing $\omega_k^N = \sqrt{\vec{k}^2 + m_N^2}$ by $\omega_k = \sqrt{\vec{k}^2 + M^2}$ in Eq. (28) (dashed line) and (33) (solid line) for the fixed values of $\vec{k} = 0$, $\mu_N = 0$ and $T = 0.150$ GeV. From the sharp

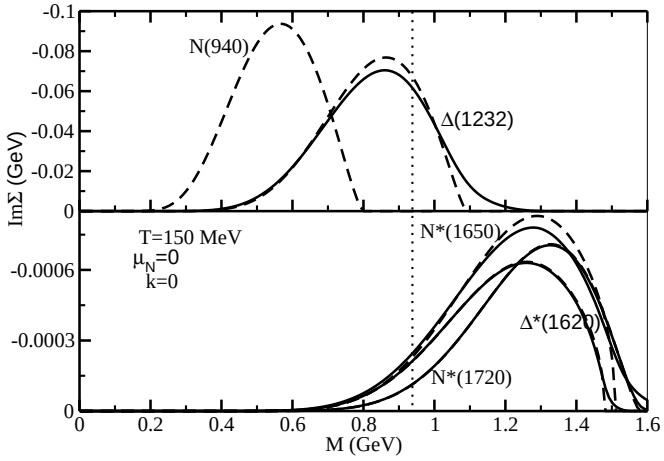

FIG. 2: Imaginary part of nucleon self-energy for different πB loops are individually shown before (dashed line) and after (solid line) folding by corresponding baryon spectral functions. $B = N(940), \Delta(1232)$ are in upper panel whereas $B = \Delta^*(1620)$, $N^*(1650), N^*(1720)$ are in lower panel for fixed values of three momentum of N ($\vec{k} = 0$), temperature ($T = 0$) and baryon chemical potential ($\mu_N = 0$).

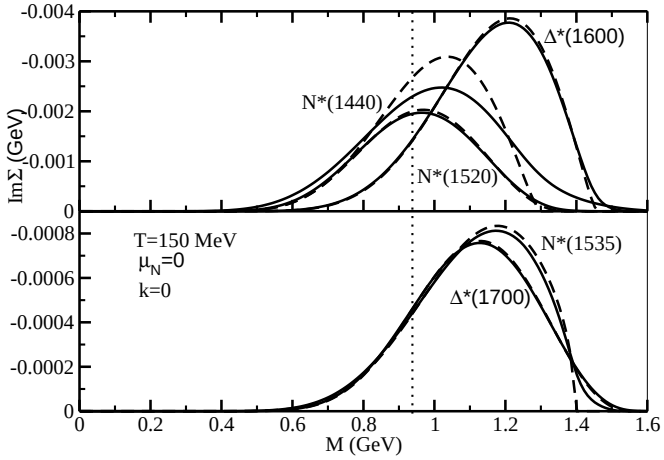

FIG. 3: Same as Fig. (2) for the rest of the baryons $B = N^*(1440)$, $N^*(1520)$, $\Delta^*(1600)$ (upper panel) and $B = N^*(1535)$, $\Delta^*(1700)$ (lower panel).

ending of the dashed line, the Landau regions for different loops are clearly visible. As an example for πN loop the Landau region is $M = 0$ to $m_N - m_\pi$, *i.e.*, 0 to 0.8 GeV. Due to the folding of the baryon spectral functions, these sharp endings are smeared towards higher value of M. Since $\Sigma^R(M)$ also depends on T, μ_N and $\vec{k}$ therefore total contribution of $\Sigma^R(M)$ from all the loops has been shown in Fig. (4) for different sets of T, μ_N and $\vec{k}$.

The nucleon thermal width Γ_N is basically the contribution of $\mathrm{Im}\Sigma^R$ at $M = m_N$, which is marked by dotted line. Being an on-shell quantity, Γ_N is associated with the thermodynamical probability of different

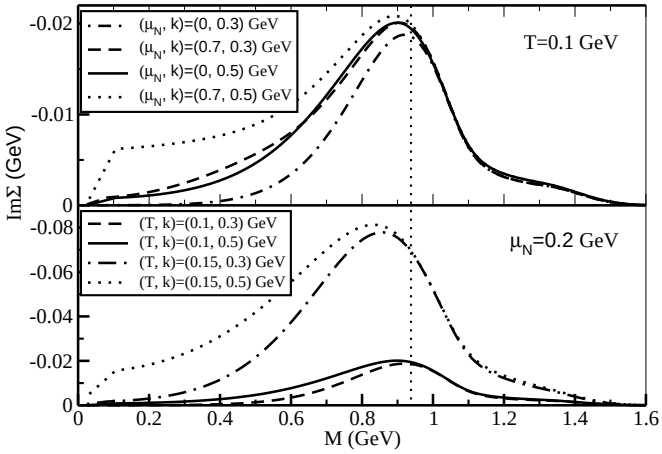

FIG. 4: Imaginary part of total self-energy for different sets of nucleon momentum ($\vec{k}$), temperature (T) and baryon chemical potential (μ_N).

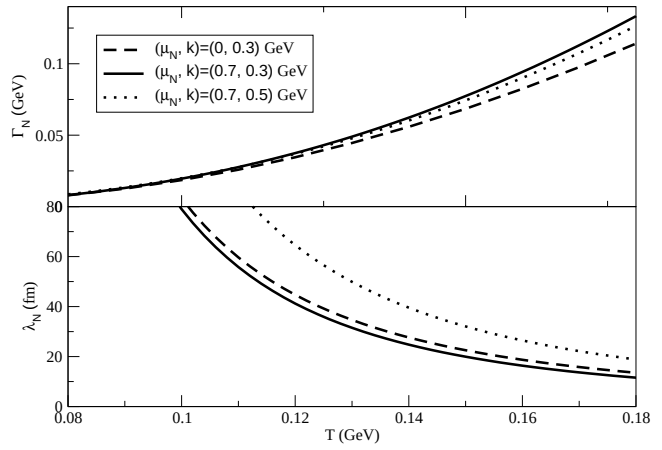

FIG. 5: The variation of nucleon thermal width Γ_N (upper panel) and its corresponding mean free path λ_N (lower panel) with T are shown.

on-shell scattering processes instead of off-shell scattering processes as described by Weldon for the imaginary part of self-energy in Ref. [52]. Following Weldon's prescription, forward and inverse scattering of nucleon can be respectively described as follows. During propagation of N, it can disappear by absorbing a thermalized π from the medium to create a thermalized B. Again N can appear by absorbing a thermalized B from the medium as well as by emitting a thermalized π. The $n_l(1 - n_u^+)$ and $n_u^+(1 + n_l)$ are the corresponding statistical probabilities of the forward and inverse scattering respectively [52], because just by adding them, we will get the thermal distribution part of Eq. (28), *i.e.*, $(n_l + n_u^+)$.

From Eq. (28) or (33), we see that Γ_N depends on temperature T, baryon chemical potential μ_N and three momentum $\vec{k}$ of nucleon. The upper panels of Fig. (5)

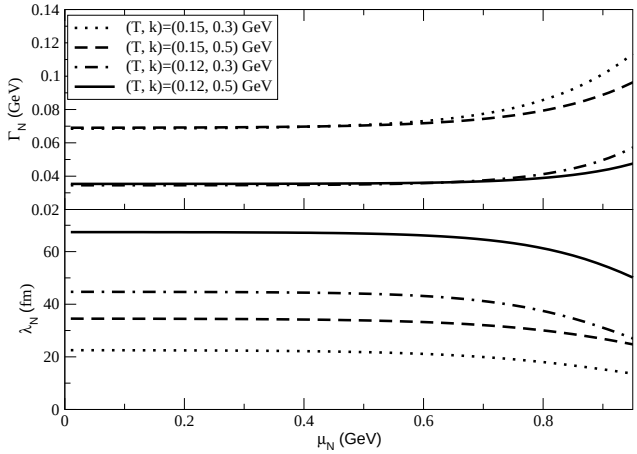

FIG. 6: The variation of nucleon thermal width Γ_N (upper panel) and its corresponding mean free path λ_N (lower panel) as a functions of baryon chemical potential μ_N are shown.

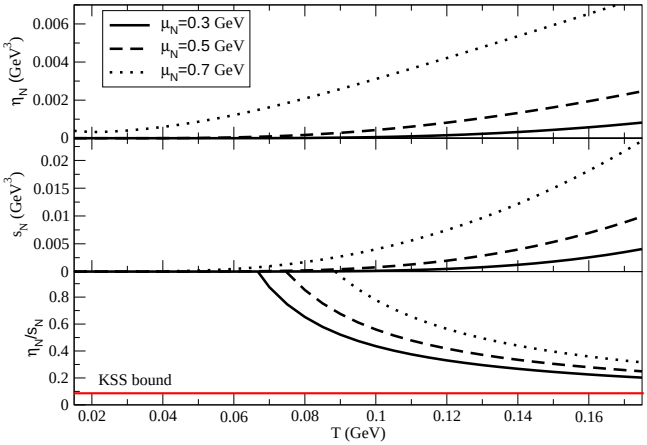

FIG. 7: (color on-line) The T dependence of η_N (upper panel), s_N (middle panel) and η_N/s_N (lower panel) of the nucleonic component. The straight red line denotes the KSS bound.

and (6) are, respectively, displaying the variation of Γ_N with T for different sets of $(\vec{k},\ \mu_N)$ and of Γ_N with μ_N for different set of $(\vec{k}, T)$. The mean free path can be defined as $\lambda_N(\vec{k}, T, \mu_N) = \frac{\vec{k}}{\omega_k^N \Gamma_N(\vec{k},T,\mu_N)}$ and its corresponding variation with T and μ_N are respectively shown in the lower panels of Fig. (5) and (6). The range of T and μ_N, in which λ_N is smaller than the dimension of the medium ($\sim 10 - 40$ fm, a typical dimension of strongly interacting matter, produced in the laboratories of HIC), plays the main role of dissipation via scattering in the medium because the larger λ is associated with the scenario after freeze out of the medium. From the dashed line of Fig. (5) we see that $T > 0.120$ GeV (but up to $T_c \approx 0.175$ GeV) is that relevant region for baryon free nuclear matter ($\mu_N = 0$). Whereas for finite baryon chemical potential (e.g. solid line of Fig. (5) at $\mu_N = 0.7$ GeV), this relevant T region will be shifted slightly toward lower temperature (in addition, T_c is also expected to decrease with increase of μ_N). Since high momentum $(\vec{k})$ of constituent particles always helps them to freeze out from the medium, the relevant T region for nucleon with high $\vec{k}$ is reduced by shifting towards the high T region. This can be understood by comparing the solid and dotted lines in the lower panel of Fig. (5).

Using the numerical function $\Gamma_N(\vec{k}, T, \mu_N)$ in Eq. (23), we get η_N as a function of T and μ_N, which are shown in the upper panels of Fig. (7) and (8). Here we see η_N is monotonically increasing with T and μ_N both. Using the simple equilibrium expression of entropy density (s_N) for nucleons,

$$s_N = 4\beta \int \frac{d^3\vec{k}}{(2\pi)^3} \left(\omega_k^N + \frac{\vec{k}^2}{3\omega_k^N} - \mu_N \right) n_k^+(\omega_k^N), \quad (35)$$

the η_N/s_N has been generated as a function of T and μ_N. From the lower panels of Fig. (7) and (8), we see

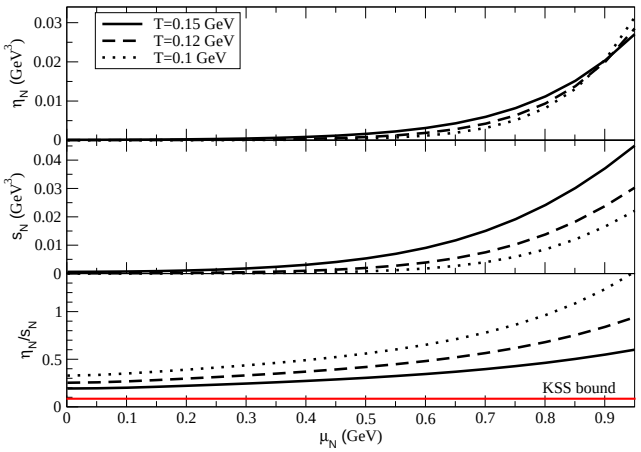

FIG. 8: (color on line) The variation of η_N (upper panel), s_N (middle panel) and η_N/s_N (lower panel) of the nucleonic component with μ_N.

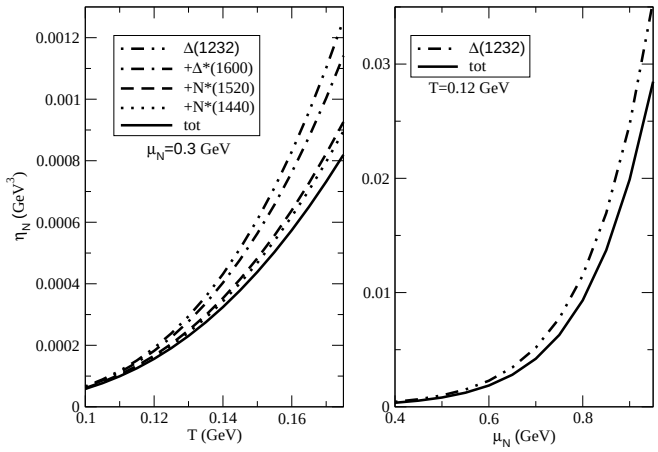

FIG. 9: The contributions of different πB loops in $\eta_N(T)$ (left panel) and $\eta_N(\mu_N)$ (right panel).

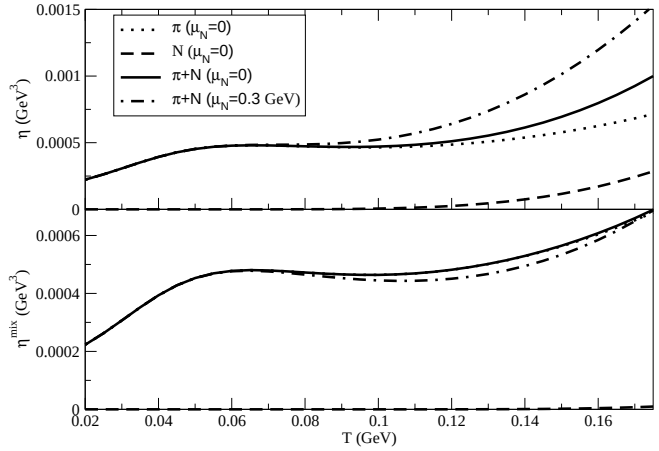

FIG. 10: The T dependence of shear viscosity for pionic (dotted line), nucleonic (dashed line) components and their total at $\mu_N = 0$ (solid line) and $\mu_N = 0.3$ GeV (dash-dotted line). The upper and lower panel contain the results without and with mixing effect, obtained from Eq.(38) and (39) respectively.

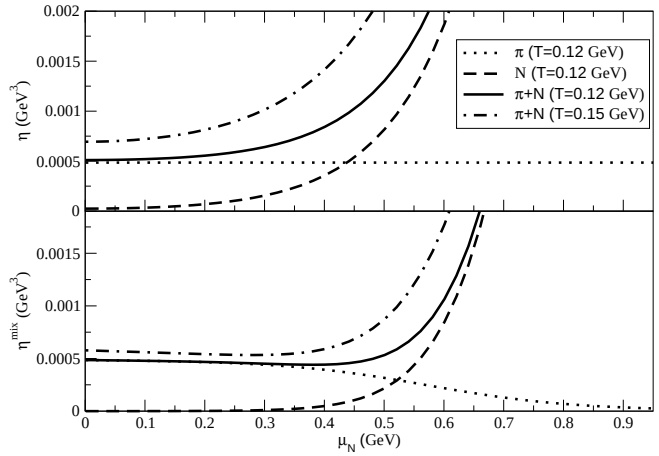

FIG. 11: Corresponding results of Fig. (10) against the μ_N axis with two different temperatures.

that η_N/s_N can be reduced by increasing T as well as by decreasing μ_N.

In the left and right panels of Fig. (9), the contributions of different loops (dominating loops only) are individually shown in η_N vs T and η_N vs μ_N graphs respectively. The $\pi\Delta$ loop plays a leading role to generate the typical values $(0.0001 - 0.01$ GeV$^3)$ of η_N for strongly interacting matter because the major part of the nucleon thermal width is coming from this loop only.

Up to now, we have calculated the contribution of shear viscosity from nucleon thermal width, although a major contribution comes from the thermal width of pion. Hence, one should add the pionic contribution with nucleon contribution for getting total shear viscosity of nuclear matter at finite temperature and density. In our recent work [53], the shear viscosity, coming from pionic thermal width has already been addressed. The one-loop Kubo expression of shear viscosity and ideal expression of entropy density for pionic components are respectively given below,

$$\eta_\pi = \frac{\beta}{10\pi^2}\int \frac{d^3k\,\vec{k}^6}{\Gamma_\pi \omega_k^{\pi 2}}\, n_k(\omega_k^\pi)\left[1 + n_k(\omega_k^\pi)\right] \ , \tag{36}$$

and

$$s_\pi = 3\beta \int \frac{d^3\vec{k}}{(2\pi)^3}\left(\omega_k^\pi + \frac{\vec{k}^2}{3\omega_k^\pi}\right) n_k(\omega_k^\pi) \ , \tag{37}$$

where $n_k(\omega_k^\pi) = 1/\{e^{\beta\omega_k^\pi} - 1\}$ is the Bose-Einstein distribution function of pion with $\omega_k^\pi = (\vec{k}^2 + m_\pi^2)^{1/2}$, and Γ_π is the thermal width of π mesons in the medium due to $\pi\sigma$ and $\pi\rho$ fluctuations.

Now, adding that pion contribution with the nucleon, one can simply get the total shear viscosity of nuclear matter as

$$\eta_{\rm tot} = \eta_\pi + \eta_N \ , \tag{38}$$

where η_π and η_N do not face any mixing effect of pion density, $\rho_\pi = 3\int \frac{d^3k}{(2\pi)^3} n_k(\omega_k^\pi)$ and nucleon density, $\rho_N = 4\int \frac{d^3k}{(2\pi)^3} n_k^+(\omega_k^N)$. However, viscosity of single component gas should be different from the viscosity of that component in a mixed gas [24, 54]. To incorporate this mixing effect for rough estimation, we follow the approximated relation [24, 54]

$$\eta_{\rm tot}^{\rm mix} = \eta_\pi^{\rm mix} + \eta_N^{\rm mix} \ , \tag{39}$$

where

$$\eta_\pi^{\rm mix} = \frac{\eta_\pi}{1 + \left(\frac{\rho_N}{\rho_\pi}\right)\left(\frac{\sigma_{\pi N}}{\sigma_{\pi\pi}}\right)\sqrt{\frac{1+m_\pi/m_N}{2}}} \tag{40}$$

and

$$\eta_N^{\rm mix} = \frac{\eta_N}{1 + \left(\frac{\rho_\pi}{\rho_N}\right)\left(\frac{\sigma_{\pi N}}{\sigma_{NN}}\right)\sqrt{\frac{1+m_N/m_\pi}{2}}} \ . \tag{41}$$

For simplicity, the cross sections of all kinds of scattering are taken as constant with same order of magnitude (*i.e.* $\sigma_{\pi\pi} \approx \sigma_{\pi N} \approx \sigma_{NN}$). In the upper panels of Fig. (10) and (11), the T and μ_N dependence of η_π (dotted line), η_N (dashed line) and their total $\eta_{\rm tot}$ (solid line and dash-dotted line for two different values of μ_N and T) are separately shown. Whereas lower panel of the figures show their corresponding mixing effect following from Eq. (40), (41) and (39). From the Fig. (11), one should notice that the independent nature of $\eta_\pi(\mu_N)$ has been changed to a decreasing function due to mixing effect. Similar qualitative trend has been seen in Ref. [24].

The entropy density of nucleon component from Eq. (35), pion component from Eq. (37) and their total $s_{\rm tot} = s_N + s_\pi$ are individually shown in the upper panels of Fig. (12) and (13) as functions of T and

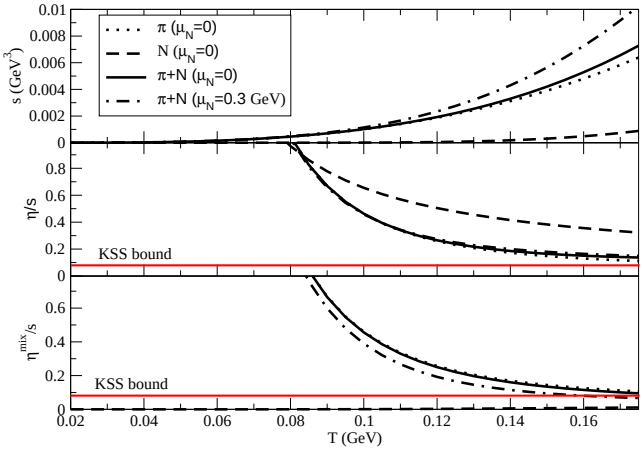

FIG. 12: (color on-line) The entropy density (upper panel), viscosity to entropy density ratio without (middle panel) and with (lower panel) mixing effect as functions of T.

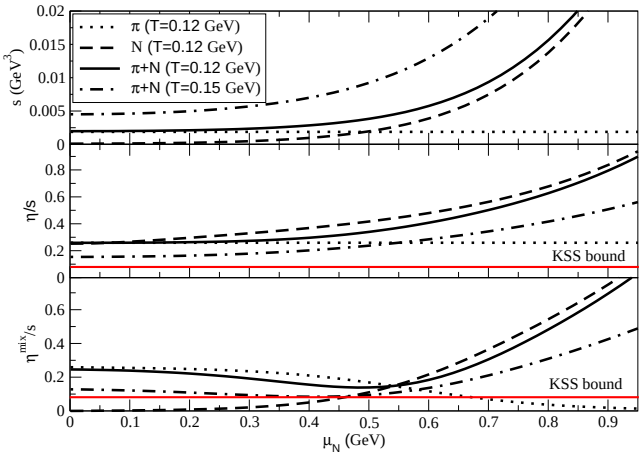

FIG. 13: (color on-line) The corresponding results of Fig. (12) are shown with respect to μ_N.

μ_N respectively. The corresponding η/s without (middle panel) and with (lower panel) mixing effect are shown in Fig. (12) and (13) as a function of T and μ_N respectively. The decreasing nature of total $\eta/s(T)$ qualitatively remains the same after incorporating the mixing effect whereas an increasing function of the total $\eta/s(\mu_N)$ transforms to a decreasing function due to this mixing effect. Comparing our results with the results of Itakura et al. [24], where $\eta/s(\mu_N)$ also reduces with μ_N, the mixing effect appears to be very important. However, the total $\eta/s(\mu_N)$ in mixing scenario becomes an increasing function beyond $\mu_N \approx 0.5$ GeV because the increasing rate of $\eta_N^{\rm mix}(\mu_N)$ dominates over the decreasing rate of $\eta_\pi^{\rm mix}(\mu_N)$ in that region. Using the effective hadronic Lagrangian, the conclusion of our results should be concentrated within regions of $0.100\ {\rm GeV} < T < 0.160\ {\rm GeV}$ and $0 < \mu_N < 0.500$ GeV.

V. SUMMARY AND CONCLUSION

Owing to the Kubo relation, the shear viscosity can be expressed in terms of two point function of the viscous stress tensors at finite temperature. By using the real-time thermal field theoretical method, this two point function has been represented as NN loop diagram when the nucleons are considered as constituent particles of the medium. A finite nucleon thermal width Γ_N has been traditionally included in the nucleon propagators of the NN loop for getting a non-divergent shear viscosity η_N. This nucleon thermal width is obtained from the one-loop self-energy of nucleon at finite temperature and density. Different possible pion baryon loops are accounted to calculate the total Γ_N, which depends on the three momentum of nucleons ($\vec{k}$) as well as the medium parameters T and μ_N. Using the numerical function $\Gamma_N(\vec{k}, T, \mu_N)$, η_N and η_N/s_N are numerically generated as functions of T and μ_N. Adding the pionic contribution taken from Ref. [53] with the numerical values of the nucleonic component, we have obtained the total shear viscosity, where a gross mixing effect of two component system has been implemented. Along the temperature axis, the shear viscosity of both pion and nucleon components appear as increasing function, whereas along the μ_N axis shear viscosity of pion component changes from its constant behavior to a decreasing function due to presence of mixing effect. The total shear viscosity to entropy density ratio ($\eta_{\rm tot}^{\rm mix}/s_{\rm tot}$) for the pion-nucleon mixed gas reduces with increasing T as well as μ_N and quantitatively becomes very close to the KSS bound. This behavior indicates that $\eta_{\rm tot}^{\rm mix}/s_{\rm tot}$ tends to reach its minimum value near the transition temperature at vanishing as well as finite value of μ_N. According to these results, the finite baryon chemical potential helps the nuclear matter to come closer to its (nearly) perfect fluid nature.

Acknowledgment : The work is financially supported by Fundacao de Amparo a Pesquisa do Estado de Sao Paulo, FAPESP (Brazilian agencies) under Contract No. 2012/16766-0. I am very grateful to Prof. Gastao Krein for his academic and non-academic support during my postdoctoral period in Brazil. I would also like to thank Abhishek Mishra, Sandeep Gautam and Supriya Mondal for their useful help while writings this article.

[1] P. Romatschke and U. Romatschke, Phys. Rev. Lett. 99, 172301 (2007); M. Luzum and P. Romatschke, Phys. Rev. **C 78**, 034915 (2008).

[2] H. Song and U. W. Heinz, Phys. Lett. **B 658**, 279 (2008); Phys. Rev. **C 78**, 024902 (2008).

[3] Z. Xu, C. Greiner, and H. Stocker, Phys. Rev. Lett. 101,

082302 (2008); Z. Xu and C. Greiner, Phys. Rev. **C 79**, 014904 (2009).
[4] G. Ferini, M. Colonna, M. Di Toro, and V. Greco, Phys. Lett. **B 670**, 325 (2009); V. Greco, M. Colonna, M. Di Toro, and G. Ferini, Prog. Part. Nucl. Phys. 65, 562 (2009).
[5] A. Adare, *et al.* (PHENIX Collaboration), Phys. Rev. Lett. 98 (2007) 162301;S. S. Adler *et al.* (PHENIX Collaboration), Phys. Rev. Lett. 91, 182301 (2003).
[6] J. Adams *et al.* (STAR Collaboration), Phys. Rev. C 72, 014904 (2005).
[7] B. B. Back *et al.* (PHOBOS Collaboration), Phys. Rev. C 72, 051901(R) (2005).
[8] L. P. Csernai, J. I. Kapusta, and L. D. McLerran, Phys. Rev. Lett. 97, 152303 (2006); J.I. Kapusta arXiv:0809.3746 [nucl-th].
[9] P. Chakraborty and J. I. Kapusta Phys. Rev **C 83**, 014906 (2011).
[10] T. Hirano, M. Gyulassy Nucl. Phys. **A 769** (2006) 71.
[11] P. Zhuang, J. Hufner, S. P. Klevansky, L. Neise Phys. Rev. **D 51** (1995) 3728; P. Rehberg, S. P. Klevansky, J. Hufner, Nucl. Phys. **A 608** (1996) 356.
[12] J. W. Chen, M. Huang, Y. H. Li, E. Nakano, D. L. Yang, Phys. Lett. **B 670** (2008) 18; J. W. Chen, C. T. Hsieh, H. H. Lin, Phys. Lett. **B 701** (2011) 327.
[13] P. Kovtun, D. T. Son, and O. A. Starinets, Phys. Rev. Lett. 94, 111601 (2005).
[14] H. Niemi, G.S. Denicol, P. Huovinen, E. Molnar, D.H. Rischke, Phys. Rev. Lett. 106 (2011) 212302.
[15] C. Shen and U. W. Heinz, Phys. Rev. **C 83**, 044909 (2011); H. Song and U. W. Heinz, Phys. Rev. **C 81**, 024905 (2010).
[16] J. R. Bhatt, H. Mishra, and V. Sreekanth, J. High Energy Phys. 11 (2010) 106.
[17] J. Peralta-Ramos, G. Krein, Int. J. Mod. Phys. Conf. Ser. 18 (2012) 204; Phys. Rev. **C 84** (2011) 044904.
[18] A. Wiranata, V. Koch, M. Prakash, X. N. Wang, Phys.Rev. C88 (2013) 4, 044917; A. Wiranata, M. Prakash, Phys. Rev. **C 85**, 054908 (2012).
[19] J. N. Hostler, J. Noronha, C. Greiner, Phys. Rev. **C 86** (2012) 024913; Phys. Rev. Lett. 103, 172302 (2009).
[20] A. S. Khvorostukhin, V. D. Toneev, D.N. Voskresensky, Phys. Atom. Nucl. 74 (2011) 650; Nucl.Phys. **A 845** (2010) 106; Nucl.Phys. A915 (2013) 158.
[21] M. Buballa, K. Heckmann, J. Wambach, Prog. Part. Nucl. Phys. 67 (2012) 348.
[22] A. Dobado and S.N. Santalla, Phys. Rev. **D 65**, 096011 (2002); A. Dobado and F. J. Llanes-Estrada, Phys. Rev. **D 69**, 116004 (2004).
[23] J. W. Chen, Y. H. Li, Y. F. Liu, and E. Nakano, Phys. Rev. **D 76**, 114011 (2007); E. Nakano, arXiv:hep-ph/0612255.
[24] K. Itakura, O. Morimatsu, and H. Otomo, Phys. Rev. **D 77**, 014014 (2008).
[25] A. Muronga, Phys. Rev. **C 69**, 044901 (2004).
[26] D. Fernandez-Fraile and A. Gomez Nicola, Eur. Phys. J. **C 62**, 37 (2009); Eur. Phys. J. A **31**, 848 (2007); Int. J. Mod. Phys. **E 16** (2007) 3010.
[27] R. Lang, N. Kaiser and W. Weise, Eur. Phys. J. **A 48**, 109 (2012); R. Lang, W. Weise, Eur. Phys. J. **A 50**, 63 (2014)
[28] S. Mitra, S. Ghosh, and S. Sarkar Phys. Rev. **C 85**, 064917 (2012).
[29] S. Pal, Phys. Lett. **B 684** (2010) 211.
[30] M. I. Gorenstein, M. Hauer, O. N. Moroz, Phys. Rev. **C 77**, 024911 (2008).
[31] G.S. Denicol, C. Gale, S. Jeon, J. Noronha, Phys. Rev. **C 88** (2013) 064901.
[32] N. Demir and S. A. Bass, Phys. Rev. Lett. 102, 172302 (2009).
[33] D. Q. Fang, Y. G. Ma, C. L. Zhou, Phys. Rev. **C 89**, 047601 (2014);
[34] N. Sadooghi, F. Taghinavaz, Phys. Rev. **D 89**, 125005 (2014).
[35] S. Gavin, Nucl. Phys. **A 435** (1985) 826
[36] M. Prakash, M. Prakash, R. Venugopalan, and G. Welke, Phys. Rep. 227, 321 (1993).
[37] J.L. Anderson, H.R. Witting, Physica 74 (1973) 466; Physica 74 (1973) 489.
[38] V.M. Galitsky, Yu.B. Ivanov, V.A. Khangulian, Sov. J. Nucl. Phys. 30 (1979) 401.
[39] P. Danielewicz, Phys. Lett. B 146 (1984) 168.
[40] R. Hakim, L. Mornas, P. Peter, H.D. Sivak, Phys. Rev. D 46 (1992) 4603; R. Hakim, L. Mornas, Phys. Rev. C 47 (1993) 2846.
[41] D. N. Zubarev *Non-equilibrium statistical thermodynamics* (New York, Consultants Bureau, 1974).
[42] R. Kubo, J. Phys. Soc. Jpn. 12, 570 (1957).
[43] A. J. Niemi and G. W. Semenoff, Annals of Physics 152, 105 (1984).
[44] S. Mallik, S. Sarkar Eur.Phys.J. **C 61** (2009) 489.
[45] A. Hosoya, M. Sakagami, and M. Takao, Ann. Phys. 154, 229 (1984).
[46] S. Ghosh, Int. J. Mod. Phys. **A 29** (2014) 1450054.
[47] M. Post, S. Leupold, U. Mosel, Nucl. Phys. **A 741**, 81 (2004).
[48] S. Ghosh, S. Sarkar, S. Mallik, Phys. Rev. **C 82** (2010) 045202.
[49] S. Ghosh and S. Sarkar, Nucl. Phys. **A 870871** (2011) 94111.
[50] S. Ghosh and S. Sarkar, Eur. Phys. J. A 49, 97 (2013).
[51] J. Beringer *et al.* (*Particle Data Group*) Phys. Rev. **D 86**, 010001 (2012).
[52] H.A. Weldon, Phys. Rev. **D 28**, 2007 (1983).
[53] S. Ghosh, G. Krein, S. Sarkar, Phys. Rev. **C 89** (2014) 045201.
[54] E. H. Kennard, *Kinetic Theory of Gases, with an Introduction to Statistical Mechanics* (McGraw-Hill, New York, 1938).